Flexural behavior of ECC-concrete composite beams reinforced with steel bars

Wen-Jie Ge[1*], Ashraf F. Ashour[2], Xiang Ji[3], Chen Cai[4], Da-Fu Cao[5]

(1. Ph.D., Associate Professor, College of Civil Science and Engineering, Yangzhou University, Yangzhou 225127, China (corresponding author), E-mail: gewj@yzu.edu.cn; 2. Ph.D., Professor, School of Engineering, University of Bradford, Bradford, BD7 1DP, UK; 3. M.S. Candidate, College of Civil Science and Engineering, Yangzhou University, Yangzhou 225127, China; 4. M.S. Candidate, College of Civil Science and Engineering, Yangzhou University, Yangzhou 225127, China; 5. M.S., Professor, College of Civil Science and Engineering, Yangzhou University, Yangzhou 225127, China.)

Abstract: This paper presents analytical technique and simplified formulas for the calculations of cracking, yield and ultimate moments of different cases as well as deflections of ECC-concrete composite beams reinforced with steel bars. The technique is based on the simplified constitutive models of materials, strain compatibility, perforce bond of materials and equilibrium of internal forces and moment. Experimental testing of eleven ECC-concrete composite beams reinforced with steel bars is also presented. All beams tested had the same geometrical dimensions but different steel reinforcement strength and ECC thickness. The proposed formulas showed good agreement with the experimental results of various moment values and deflections. A parametric analysis shows that yield and ultimate moments increase with the increase of concrete strength in case of compression failure but, essentially, remain unchanged in case of tensile failure. With increasing the tensile resistance, for example by increasing ECC height replacement ratio, reinforcement ratio, strength of steel reinforcement and ECC, ultimate curvature and energy dissipation increase in case of tensile failure and decrease in case of compressive failure. On the other hand, ductility and energy dissipation ratio decrease with the increase of reinforcement ratio and strength, but, essentially, remain unchanged with increasing the height replacement ratio and strength of ECC.

Keywords: ECC; concrete; composite beams; flexural behavior; ductility; deflection; energy dissipation.

1 Introduction

Under the combined effects of mechanical loads and environmental exposure, many reinforced concrete structures deteriorate due to steel corrosion and cannot meet the requirement of ultimate limit state and durability. Therefore, repair and rehabilitation of such structures have become a large part of construction activity.

During the last decade, concrete technology has been undergoing rapid development, resulting in the production of a new concept of engineered cementitious composite (ECC) to overcome the brittle behavior of cement-based materials. ECC exhibits multiple micro cracks, leading to a significant increase in strain capacity and ductile behavior. It has also excellent toughness and energy absorption capacity [1], self-healing ability [2, 3], fire performance [4], remains durable under erosion

environment (sulfate-chloride environment [2], freezing-thawing and sulfate coupling environment [5]).

Few investigations were devoted to improve the performance of ECC, such as hybridization with non-round polypropylene fiber and low modulus polyvinyl alcohol fiber [6], incorporating $CaCO_3$ whisker to improve compressive strength and tensile strain-hardening [7], increasing slag content improved the ductility, hardened air content, water absorption, porosity and sorptivity [5], using recycled concrete fines as microsilica sand substitute in the production of ECC [8], incorporating high volumes of fly ash and micro PVA fibers to improve the cyclic freeze-thaw resistance and microstructure of ECC [3, 9], adding waterproofing admixture to improve wetting property and reduce the sorptivity, and shrinkage-reducing admixture together with calcium sulfoaluminate cement to control the drying shrinkage[10].

Experimental study showed that the use of ECC in the tensile zone around longitudinal steel reinforcement has slightly improved both the flexural capacity [11-13] and deformation ability [12, 13], but significantly reduced the crack width before yielding of steel reinforcement [12]. Therefore, durability of composite ECC/reinforced concrete elements can be greatly improved due to the enhancement of waterproof and corrosion resistance [14-16]. A theoretical analysis of bending resistance of ECC-RC composite beams was developed and it is compared well with the experimental results [17, 18]. On the other hand, when the ECC thickness increased beyond a certain critical value, both the flexural strength and ductility of ECC-concrete composite beams significantly enhanced [19, 20].

Because of its excellent tensile performance, ECC can be used in strengthening unreinforced masonry walls [16, 21-23], reducing the extensive amount of transverse reinforcements in beam-column joints of rigid-framed bridges, enhancing the joint seismic resistance and reducing reinforcement congestion and construction complexity [24-27]. ECC can also be used in hydraulic structures for its good durability [2, 16, 28], highway engineering for its ability of withstanding large deformations from heavy loading and temperature variations [29], in hot arid coastal climatic condition structures [30], in lightweight building facade and pavement [31], in pavement overlay to extend the service life [32] and in impact and blast resistant protective panels [16]. The wide range of applications of ECC demonstrates that incorporating ECC can significantly improve the performance of structures and reduce the associated life cycle cost.

Theoretical analysis covering the whole loading process of composite beams is still limited. Based on simplified constitutive models of materials and equilibrium of internal forces and moments, mechanical behavior of composite beams is predicted below. Physical flexural testing of ECC-concrete composite beams reinforced with different ECC height replacement ratio and strength of steel reinforcement were also conducted, that is used to validate the developed analytical analysis. Experimental study shows that compared with normal concrete beam, ECC-concrete composite beam has slightly improved both the flexural capacity and deformation ability, significantly reduced the crack width before yielding of steel reinforcement, agreeing with the results obtained by reference [11-13]. A detailed parametric study is, then, carried out to establish the variation of mechanical behavior (yield moment, ultimate moment, ultimate curvature, ductility, energy disspation and energy dissipation ratio)

of composite beams with the main influential parameters (such as ECC height replacement ratio, reinforcement ratio, strength of steel reinforcement, concrete and ECC). Parametric study shows that, with increasing the ECC height replacement ratio, ultimate curvature increases in case of tensile failure, this result similar to the trend observed in reference [19, 20], but decreases in case of compressive failure. Calculate formula of cracking, yield moment ultimate moment and deflections of ECC-concrete composite beams as well as the results obtained from the experimental and parametric study can be taken as reference in practice application.

2 Constitutive models of materials

(1) Steel reinforcement

The constitutive relationships of steel bars in tension and compression are simplified to a bilinear model as shown in figure 1 [33], where ε_s and σ_s are the tensile strain and stress in steel bar, respectively, ε_{sy} and f_{sy} are the yield strain and stress, respectively, E_s is the elastic modulus and ε_{su} is the ultimate tensile strain (assumed to be 0.01).

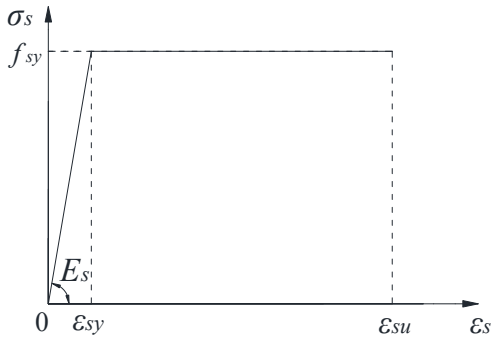

Fig.1 Constitutive relationships of steel bar

(2) Concrete

The compressive stress-strain curve of concrete [33] is shown in figure 2(a) and can be expressed by:

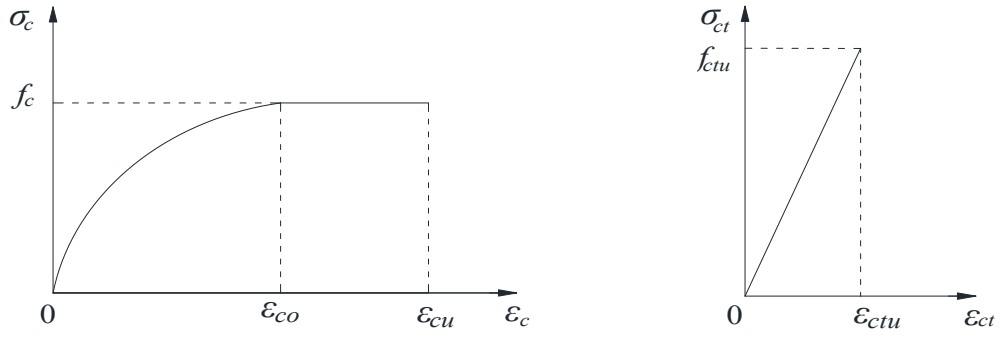

(a) Compression (b) Tension

Fig.2 Constitutive relationships of concrete

$$\sigma_c = \begin{cases} f_c(1-(1-\varepsilon_c/\varepsilon_{co})^n) & ,0 \le \varepsilon_c \le \varepsilon_{co} \\ f_c & ,\varepsilon_{co} < \varepsilon_c \le \varepsilon_{cu} \end{cases} \quad (1)$$

$$n = 2\text{-}(f_{cu,k}\text{-}50)/60 \quad (2)$$

$$\varepsilon_{co} = 0.002+0.5(f_{cu,k}\text{-}50)\times 10^{-5} \quad (3)$$

$$\varepsilon_{cu} = 0.0033\text{-}0.5(f_{cu,k}\text{-}50)\times 10^{-5} \quad (4)$$

where ε_c and σ_c are the compressive strain and stress in concrete, respectively, f_c is the concrete compressive strength, ε_{co} (≥ 0.002) is the compressive strain corresponding to concrete stress of f_c, ε_{cu} (≤ 0.0033) is the ultimate compressive strain of concrete, $f_{cu,k}$ is the concrete cube compressive strength and n (≤ 2.0) is a coefficient related to the compressive stress-strain relationship of concrete.

The concrete uniaxial tensile stress-strain model is shown in figure 2(b) and can be represented by the following equation.

$$\sigma_{ct} = \begin{cases} f_{ctu}\varepsilon_{ct} / \varepsilon_{ctu} & ,0 \leq \varepsilon_{ct} \leq \varepsilon_{ctu} \\ 0 & ,\varepsilon_{ct} > \varepsilon_{ctu} \end{cases} \tag{5}$$

where ε_{ct} and σ_{ct} are the tensile strain and stress in concrete, respectively, ε_{ctu} and f_{ctu} are the ultimate uniaxial tensile strain and stress, respectively.

(3) ECC

The compressive stress-strain curve [34] of ECC is shown in figure 3(a) and can be formulated by:

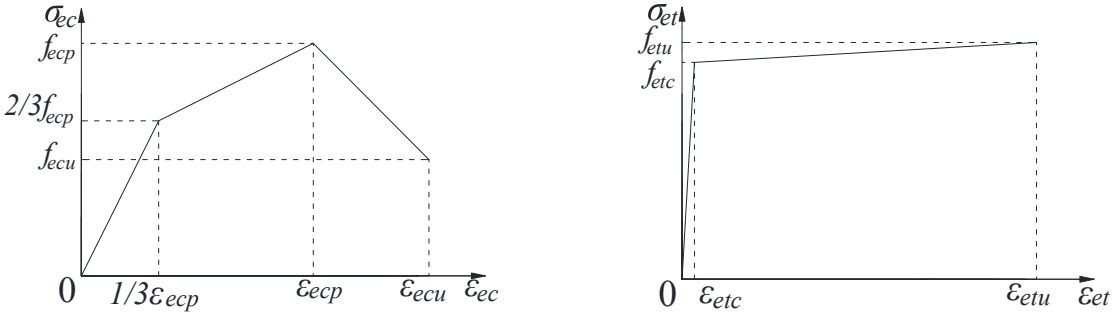

(a) Compression (b) Tension

Fig.3 Constitutive relationships of ECC

$$\sigma_{ec} = \begin{cases} 2f_{ecp}/\varepsilon_{ecp}\varepsilon_{ec} & ,0 \leq \varepsilon_{ec} \leq \varepsilon_{ecp}/3 \\ 2f_{ecp}/3 + f_{ecp}/(2\varepsilon_{ecp})(\varepsilon_{ec} - \varepsilon_{ecp}/3) & ,\varepsilon_{ecp}/3 < \varepsilon_{ec} \leq \varepsilon_{ecp} \\ f_{ecp} + (f_{ecu} - f_{ecp})/(\varepsilon_{ecu} - \varepsilon_{ecp})(\varepsilon_{ec} - \varepsilon_{ecp}) & ,\varepsilon_{ecp} < \varepsilon_{ec} \leq \varepsilon_{ecu} \end{cases} \tag{6}$$

where ε_{ec} and σ_{ec} are the compressive strain and stress in ECC, respectively, f_{ecp} and ε_{ecp} are the compressive strength (peak point of the curve) and corresponding strain, respectively, f_{ecu} and ε_{ecu} are the ultimate compressive stress (after peak point) and corresponding strain, respectively. In this paper, it is assumed that $f_{ecu} = 0.5\, f_{ecp}$ and $\varepsilon_{ecu} = 1.5\, \varepsilon_{ecp}$ [34].

The tensile stress-strain curve [14] of ECC is shown in figure 3(b) and can be expressed by the following equation.

$$\sigma_{et} = \begin{cases} f_{etc}/\varepsilon_{etc}\varepsilon_{et} & ,0 \leq \varepsilon_{et} \leq \varepsilon_{etc} \\ f_{etc} + (f_{etu} - f_{etc})/(\varepsilon_{etu} - \varepsilon_{etc})(\varepsilon_{et} - \varepsilon_{etc}) & ,\varepsilon_{etc} < \varepsilon_{et} \leq \varepsilon_{etu} \end{cases} \tag{7}$$

where ε_{et} and σ_{et} are the tensile strain and stress in ECC, respectively, ε_{etc} and f_{etc} are the tensile strain at first cracking and corresponding stress, respectively, ε_{etu} and f_{etu} are the ultimate tensile strain and corresponding stress, respectively.

3 Cross-section analysis of composite beams

The analysis below is developed for a rectangular beam section; however, it can be easily modified for other section shapes. The following assumptions have been

considered:

- The steel bars and concrete/ECC have perfect bond and no delamination between ECC and concrete is considered as observed in experimental investigations [35].
- Each plane cross section perpendicular to the axis of the beam remains plane after loading.
- The whole loading process can be divided into three stages:

1. Elastic stage (uncracked section): from being loading to cracking (ECC or concrete).

2. Working stress stage: from cracking to yielding of steel bars.

3. Failure stage: from yielding of steel bars to failure of composite beams (i.e. any material reaches its ultimate strain: (a). Compressive strain in concrete reaches ε_{cu}. (b). Tensile strain in steel bars reaches ε_{su}. (c). Tensile strain in ECC reaches ε_{etu}).

The cross-section stress-strain distributions of each loading stage are shown in figure 4, where b and h are the width and height of cross-section, respectively, h_s is the distance of the center of steel bars to the cross-section tensile edge, h_e is the thickness of ECC, h_t is the height of cross-section part in tension (neutral axis depth), x is the vertical distance of any point to the tensile edge of cross-section, ε_{et} is the maximum tensile strain in ECC, ε_{ct} and ε_c are the maximum tensile and compressive strain in concrete, respectively, ε_s is the tensile strain in steel bars and h_p is the vertical distance of concrete where its strain reaches ε_{co} to the tensile edge of cross-section, $h_p = h_t(1+\varepsilon_{co}/\varepsilon_{et})$.

The cross-section strain distribution can be expressed as:

$$\varepsilon(x) = \begin{cases} (1 - x / h_t)\varepsilon_{et} & ,0 \le x \le h_t \\ (x / h_t - 1)\varepsilon_{et} & ,h_t < x \le h \end{cases} \tag{8}$$

When $x = h_s$, the strain and stress in steel bars are $\varepsilon_s = \varepsilon_{et}(h_t-h_s)/h_t$ and $\sigma_s = E_s\varepsilon_{et}(h_t-h_s)/h_t$, respectively, but $\sigma_s = f_{sy}$ when $\varepsilon_s \ge \varepsilon_{sy}$.

According to force equilibrium of cross-section, $\sum N = 0$, the following equation can be obtained.

$$\int_0^{h_e} \sigma(x)bdx + \int_{h_e}^{h_t} \sigma(x)bdx + \sigma_s A_s - \int_{h_t}^{h} \sigma(x)bdx = 0 \tag{9}$$

Substituting stress and strain into Eq. (9), then the neutral axis depth h_t can be obtained as presented in table 1 for different stages of loading and failure. Therefore, the neutral axis depth h_t can be calculated for each value of ε_{et}. According to the moment equilibrium of cross-section, $\sum M = 0$, the cross-section moment can, then, be obtained from:

$$M = \int_{h_t}^{h} \sigma(x)bxdx - \int_0^{h_e} \sigma(x)bxdx - \int_{h_e}^{h_t} \sigma(x)bxdx - \sigma_s A_s h_s \tag{10}$$

The cross-section analysis of composite beams in different stages are shown in figure 4 and table 1, including strains, stresses in concrete and ECC, neutral axis depth and moment for each stage.

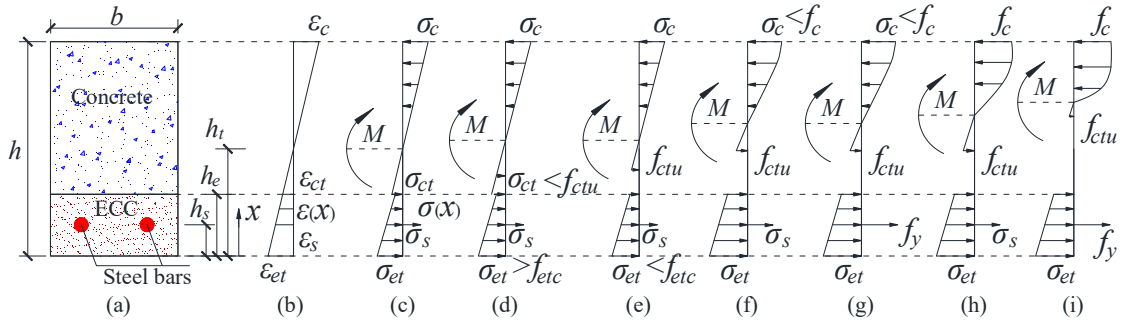

Fig.4 Cross-section stress-strain distribution of each stage: (a) beam cross section; (b) strain distribution; (c) to (i) stress distribution for various loading stages as explained in table 1

Table 1 Cross-section analyses of composite beams in different stages

(1) Elastic stage (uncracked section) (Fig.4 (c))	
Strain	$\varepsilon_c < \varepsilon_{co}$, $\varepsilon_{et} < \varepsilon_{etc}$, $\varepsilon_{ct} < \varepsilon_{ctu}$, $\varepsilon_s = \varepsilon_{et}(h_t-h_s)/h_t < \varepsilon_{sy}$
Stress in concrete /ECC	$\sigma(x)=\begin{cases} f_{etc}/\varepsilon_{etc}\varepsilon(x) & ,0\le x\le h_e \\ f_{ctu}/\varepsilon_{ctu}\varepsilon(x) & ,h_e<x\le h_t \\ f_c(2\varepsilon(x)/\varepsilon_{co}-\varepsilon(x)^2/\varepsilon_{co}^2) & ,h_t<x\le h \end{cases}$ (11)
Neutral axis depth	$h_t^3(\frac{f_{ctu}}{2\varepsilon_{ctu}}-\frac{f_c}{\varepsilon_{co}}-\frac{f_c\varepsilon_{et}}{3\varepsilon_{co}^2})+h_t^2(\frac{f_{etc}h_e}{\varepsilon_{etc}}-\frac{f_{ctu}h_e}{\varepsilon_{ctu}}+\frac{E_sA_s}{b}+\frac{2f_ch}{\varepsilon_{co}}+\frac{f_ch\varepsilon_{et}}{\varepsilon_{co}^2})$ $+h_t(-\frac{f_{etc}h_e^2}{2\varepsilon_{etc}}+\frac{f_{ctu}h_e^2}{2\varepsilon_{ctu}}-\frac{E_sA_sh_s}{b}-\frac{f_ch^2}{\varepsilon_{co}}-\frac{f_ch^2\varepsilon_{et}}{\varepsilon_{co}^2})+\frac{f_ch^3\varepsilon_{et}}{3\varepsilon_{co}^2}=0$ (12)
Moment	$M=\frac{f_cb\varepsilon_{et}}{\varepsilon_{co}}(\frac{2h^3}{3h_t}-h^2+\frac{h_t^2}{3})-\frac{f_cb\varepsilon_{et}^2}{\varepsilon_{co}^2}(\frac{h^4}{4h_t^2}-\frac{2h^3}{3h_t}+\frac{h^2}{2}-\frac{h_t^2}{12})-$ $\frac{f_{etc}b\varepsilon_{et}}{\varepsilon_{etc}}(\frac{h_e^2}{2}-\frac{h_e^3}{3h_t})-\frac{f_{ctu}b\varepsilon_{et}}{\varepsilon_{ctu}}(\frac{h_t^2}{6}-\frac{h_e^2}{2}+\frac{h_e^3}{3h_t})-\frac{h_t-h_s}{h_t}\varepsilon_{et}E_sA_sh_s$ (13)
(2) Working stress stage: Case 1-ECC cracks before concrete (Fig.4 (d))	
Strain	$\varepsilon_c < \varepsilon_{co}$, $\varepsilon_{et} \ge \varepsilon_{etc}$, $\varepsilon_{ct} < \varepsilon_{ctu}$, $\varepsilon_s = \varepsilon_{et}(h_t-h_s)/h_t < \varepsilon_{sy}$
Stress in concrete /ECC	$\sigma(x)=\begin{cases} f_{etc}+(f_{etu}-f_{etc})/(\varepsilon_{etu}-\varepsilon_{etc})(\varepsilon(x)-\varepsilon_{etc}) & ,0\le x\le h_e \\ f_{ctu}\varepsilon(x)/\varepsilon_{ctu} & ,h_e<x\le h_t \\ f_c(2\varepsilon(x)/\varepsilon_{co}-\varepsilon(x)^2/\varepsilon_{co}^2) & ,h_t<x\le h \end{cases}$ (14)
Neutral axis depth	$h_t^3(\frac{f_{ctu}}{2\varepsilon_{ctu}}-\frac{f_c}{\varepsilon_{co}}-\frac{f_c\varepsilon_{et}}{3\varepsilon_{co}^2})+h_t^2(\frac{f_{etc}h_e}{\varepsilon_{et}}+\frac{f_{etu}-f_{etc}}{\varepsilon_{etu}-\varepsilon_{etc}}(h_e-h_e\frac{\varepsilon_{etc}}{\varepsilon_{et}})$ $-\frac{f_{ctu}h_e}{\varepsilon_{ctu}}+\frac{E_sA_s}{b}+\frac{2f_ch}{\varepsilon_{co}}+\frac{f_ch\varepsilon_{et}}{\varepsilon_{co}^2})+h_t(-\frac{h_e^2}{2}\frac{f_{etu}-f_{etc}}{\varepsilon_{etu}-\varepsilon_{etc}}$ $+\frac{f_{ctu}h_e^2}{2\varepsilon_{ctu}}-\frac{E_sA_sh_s}{b}-\frac{f_ch^2}{\varepsilon_{co}}-\frac{f_ch^2\varepsilon_{et}}{\varepsilon_{co}^2})+\frac{f_ch^3\varepsilon_{et}}{3\varepsilon_{co}^2}=0$ (15)
Moment	$M=\frac{f_cb\varepsilon_{et}}{\varepsilon_{co}}(\frac{2h^3}{3h_t}-h^2+\frac{h_t^2}{3})-\frac{f_cb\varepsilon_{et}^2}{\varepsilon_{co}^2}(\frac{h^4}{4h_t^2}-\frac{2h^3}{3h_t}+\frac{h^2}{2}-\frac{h_t^2}{12})-\frac{h_t-h_s}{h_t}\varepsilon_{et}E_sA_sh_s$ $+\frac{f_{etu}-f_{etc}}{\varepsilon_{etu}-\varepsilon_{etc}}bh_e^2(\frac{h_e\varepsilon_{et}}{3h_t}-\frac{\varepsilon_{et}-\varepsilon_{etc}}{2})-\frac{f_{ctu}b\varepsilon_{et}}{\varepsilon_{ctu}}(\frac{h_t^2}{6}-\frac{h_e^2}{2}+\frac{h_e^3}{3h_t})-\frac{f_{etc}bh_e^2}{2}$ (16)

(3) Working stress stage: Case 2-Concrete cracks before ECC (Fig.4 (e))	
Strain	$\varepsilon_c < \varepsilon_{co}$, $\varepsilon_{et} < \varepsilon_{etc}$, $\varepsilon_{ct} \geq \varepsilon_{ctu}$, $\varepsilon_s = \varepsilon_{et}(h_t - h_s)/h_t < \varepsilon_{sy}$
Stress in concrete /ECC	$\sigma(x) = \begin{cases} f_{etc}/\varepsilon_{etc}\varepsilon(x) & ,0 \leq x \leq h_e \\ 0 & ,h_e < x \leq h_t \\ f_c(2\varepsilon(x)/\varepsilon_{co} - \varepsilon(x)^2/\varepsilon_{co}^2) & ,h_t < x \leq h \end{cases}$ (17)
Neutral axis depth	$h_t^3(-\frac{f_c}{\varepsilon_{co}} - \frac{f_c\varepsilon_{et}}{3\varepsilon_{co}^2}) + h_t^2(\frac{f_{etc}h_e}{\varepsilon_{etc}} + \frac{E_sA_s}{b} + \frac{2f_ch}{\varepsilon_{co}} + \frac{f_ch\varepsilon_{et}}{\varepsilon_{co}^2}) + h_t(-\frac{f_{etc}h_e^2}{2\varepsilon_{etc}} - \frac{E_sA_sh_s}{b} - \frac{f_ch^2}{\varepsilon_{co}} - \frac{f_ch^2\varepsilon_{et}}{\varepsilon_{co}^2}) + \frac{f_ch^3\varepsilon_{et}}{3\varepsilon_{co}^2} = 0$ (18)
Moment	$M = \frac{f_cb\varepsilon_{et}}{\varepsilon_{co}}(\frac{2h^3}{3h_t} - h^2 + \frac{h_t^2}{3}) - \frac{f_cb\varepsilon_{et}^2}{\varepsilon_{co}^2}(\frac{h^4}{4h_t^2} - \frac{2h^3}{3h_t} + \frac{h^2}{2} - \frac{h_t^2}{12}) - \frac{f_{etc}b\varepsilon_{et}}{\varepsilon_{etc}}(\frac{h_e^2}{2} - \frac{h_e^3}{3h_t}) - \frac{h_t - h_s}{h_t}\varepsilon_{et}E_sA_sh_s$ (19)
(4) Working stress stage: Case 3- Compressive concrete in the elastic stage after cracking and steel bars not yielded (Fig.4 (f))	
Strain	$\varepsilon_c < \varepsilon_{co}$, $\varepsilon_{et} \geq \varepsilon_{etc}$, $\varepsilon_{ct} \geq \varepsilon_{ctu}$, $\varepsilon_s = \varepsilon_{et}(h_t - h_s)/h_t < \varepsilon_{sy}$
Stress in concrete /ECC	$\sigma(x) = \begin{cases} f_{etc} + (f_{etu} - f_{etc})/(\varepsilon_{etu} - \varepsilon_{etc})(\varepsilon(x) - \varepsilon_{etc}) & ,0 \leq x \leq h_e \\ 0 & ,h_e < x \leq h_t \\ f_c(2\varepsilon(x)/\varepsilon_{co} - \varepsilon(x)^2/\varepsilon_{co}^2) & ,h_t < x \leq h \end{cases}$ (20)
Neutral axis depth	$h_t^3(\frac{f_c}{\varepsilon_{co}} + \frac{f_c\varepsilon_{et}}{3\varepsilon_{co}^2}) + h_t^2(-\frac{f_{etc}h_e}{\varepsilon_{et}} - \frac{f_{etu} - f_{etc}}{\varepsilon_{etu} - \varepsilon_{etc}}(1 - \frac{\varepsilon_{etc}}{\varepsilon_{et}})h_e - \frac{E_sA_s}{b} - \frac{2f_ch}{\varepsilon_{co}} - \frac{f_ch\varepsilon_{et}}{\varepsilon_{co}^2}) + h_t(\frac{h_e^2}{2}\frac{f_{etu} - f_{etc}}{\varepsilon_{etu} - \varepsilon_{etc}} + \frac{E_sA_sh_s}{b} + \frac{f_ch^2}{\varepsilon_{co}} + \frac{f_ch^2\varepsilon_{et}}{\varepsilon_{co}^2}) - \frac{f_ch^3\varepsilon_{et}}{3\varepsilon_{co}^2} = 0$ (21)
Moment	$M = \frac{f_cb\varepsilon_{et}}{\varepsilon_{co}}(\frac{2h^3}{3h_t} - h^2 + \frac{h_t^2}{3}) - \frac{f_cb\varepsilon_{et}^2}{\varepsilon_{co}^2}(\frac{h^4}{4h_t^2} - \frac{2h^3}{3h_t} + \frac{h^2}{2} - \frac{h_t^2}{12}) - \frac{f_{etc}bh_e^2}{2} + \frac{bh_e^3\varepsilon_{et}}{3h_t}\frac{f_{etu} - f_{etc}}{\varepsilon_{etu} - \varepsilon_{etc}} - \frac{bh_e^2}{2}\frac{f_{etu} - f_{etc}}{\varepsilon_{etu} - \varepsilon_{etc}}(\varepsilon_{et} - \varepsilon_{etc}) - \frac{h_t - h_s}{h_t}\varepsilon_{et}E_sA_sh_s$ (22)
(5) Working stress stage: Case 3- Compressive concrete in the elastic stage after cracking and steel bars yielded (Fig.4 (g))	
Strain	$\varepsilon_c < \varepsilon_{co}$, $\varepsilon_{et} \geq \varepsilon_{etc}$, $\varepsilon_{ct} \geq \varepsilon_{ctu}$, $\varepsilon_s = \varepsilon_{et}(h_t - h_s)/h_t \geq \varepsilon_{sy}$
Neutral axis depth	$h_t^3(-\frac{f_c}{\varepsilon_{co}} - \frac{f_c\varepsilon_{et}}{3\varepsilon_{co}^2}) + h_t^2(\frac{f_{etc}h_e}{\varepsilon_{et}} + \frac{f_{etu} - f_{etc}}{\varepsilon_{etu} - \varepsilon_{etc}}(1 - \frac{\varepsilon_{etc}}{\varepsilon_{et}})h_e + \frac{f_{sy}A_s}{b\varepsilon_{et}} + \frac{2f_ch}{\varepsilon_{co}} + \frac{f_ch\varepsilon_{et}}{\varepsilon_{co}^2}) + h_t(-\frac{h_e^2}{2}\frac{f_{etu} - f_{etc}}{\varepsilon_{etu} - \varepsilon_{etc}} - \frac{f_ch^2}{\varepsilon_{co}} - \frac{f_ch^2\varepsilon_{et}}{\varepsilon_{co}^2}) + \frac{f_ch^3\varepsilon_{et}}{3\varepsilon_{co}^2} = 0$ (23)

Moment	$M=\frac{f_c b\varepsilon_{\text{et}}}{\varepsilon_{co}}(\frac{2h^3}{3h_t}-h^2+\frac{h_t^2}{3})-\frac{f_c b\varepsilon_{\text{et}}^2}{\varepsilon_{co}^2}(\frac{h^4}{4h_t^2}-\frac{2h^3}{3h_t}+\frac{h^2}{2}-\frac{h_t^2}{12})-\frac{f_{etc}bh_e^2}{2}$ $+\frac{bh_e^3\varepsilon_{\text{et}}}{3h_t}\frac{f_{etu}-f_{etc}}{\varepsilon_{\text{etu}}-\varepsilon_{\text{etc}}}-\frac{bh_e^2}{2}\frac{f_{etu}-f_{etc}}{\varepsilon_{\text{etu}}-\varepsilon_{\text{etc}}}(\varepsilon_{\text{et}}-\varepsilon_{\text{etc}})-f_{sy}A_s h_s$	(24)
(6) Working stress stage: Case 4- Compressive concrete in the plastic stage after cracking and steel bars not yielded (Fig.4 (h))		
Strain	$\varepsilon_{\text{c}}\geq\varepsilon_{\text{co}}$, $\varepsilon_{\text{et}}\geq\varepsilon_{\text{etc}}$, $\varepsilon_{\text{ct}}\geq\varepsilon_{\text{ctu}}$, $\varepsilon_{\text{s}}=\varepsilon_{\text{et}}(h_{\text{t}}-h_{\text{s}})/h_{\text{t}}<\varepsilon_{\text{sy}}$	
Stress in concrete /ECC	$\sigma(x)=\begin{cases}f_{etc}+(f_{etu}-f_{etc})/(\varepsilon_{\text{etu}}-\varepsilon_{\text{etc}})(\varepsilon(x)-\varepsilon_{\text{etc}}) & ,0\leq x\leq h_e\\ 0 & ,h_e<x\leq h_t\\ f_c(2\varepsilon(x)/\varepsilon_{\text{co}}-\varepsilon(x)^2/\varepsilon_{co}^2) & ,h_t<x\leq h_p\\ f_c & ,h_{\text{p}}<x\leq h\end{cases}$	(25)
Neutral axis depth	$h_t^2(f_c+\frac{f_c\varepsilon_{\text{co}}}{3\varepsilon_{\text{et}}})+h_t(f_{etc}h_e+\frac{f_{etu}-f_{etc}}{\varepsilon_{\text{etu}}-\varepsilon_{\text{etc}}}(\varepsilon_{et}-\varepsilon_{\text{etc}})h_e+$ $\frac{E_s A_s\varepsilon_{et}}{b}-f_c h)+(-\frac{\varepsilon_{et}h_e^2}{2}\frac{f_{etu}-f_{etc}}{\varepsilon_{\text{etu}}-\varepsilon_{\text{etc}}}-\frac{E_s\varepsilon_{et}A_s h_s}{b})=0$	(26)
Moment	$M=\frac{f_c bh^2}{2}-f_c bh_t^2(\frac{\varepsilon_{co}^2}{12\varepsilon_{\text{et}}^2}+\frac{1}{2}+\frac{\varepsilon_{co}}{3\varepsilon_{\text{et}}})-\frac{h_t-h_s}{h_t}\varepsilon_{\text{et}}E_s A_s h_s$ $+bh_e^2\frac{f_{etu}-f_{etc}}{\varepsilon_{\text{etu}}-\varepsilon_{\text{etc}}}(\frac{h_e\varepsilon_{\text{et}}}{3h_t}-\frac{\varepsilon_{\text{et}}}{2}+\frac{\varepsilon_{\text{etc}}}{2})-\frac{f_{etc}bh_e^2}{2}$	(27)
(6) Failure stage: Compressive concrete in the plastic stage after cracking and steel bars yielded (Fig.4 (i))		
Strain	$\varepsilon_{\text{c}}\geq\varepsilon_{\text{co}}$, $\varepsilon_{\text{et}}\geq\varepsilon_{\text{etc}}$, $\varepsilon_{\text{ct}}\geq\varepsilon_{\text{ctu}}$, $\varepsilon_{\text{s}}=\varepsilon_{\text{et}}(h_{\text{t}}-h_{\text{s}})/h_{\text{t}}\geq\varepsilon_{\text{sy}}$	
Neutral axis depth	$h_t^2(f_c+\frac{f_c\varepsilon_{\text{co}}}{3\varepsilon_{\text{et}}})+h_t(f_{etc}h_e+\frac{f_{etu}-f_{etc}}{\varepsilon_{\text{etu}}-\varepsilon_{\text{etc}}}h_e(\varepsilon_{et}-\varepsilon_{\text{etc}})$ $+\frac{f_{sy}A_s}{b}-f_c h)-\frac{h_e^2\varepsilon_{et}}{2}\frac{f_{etu}-f_{etc}}{\varepsilon_{\text{etu}}-\varepsilon_{\text{etc}}}=0$	(28)
Moment	$M=\frac{f_c bh^2}{2}-f_c bh_t^2(\frac{\varepsilon_{co}^2}{12\varepsilon_{\text{et}}^2}+\frac{\varepsilon_{co}}{3\varepsilon_{\text{et}}}+\frac{1}{2})-\frac{f_{etc}bh_e^2}{2}$ $+\frac{bh_e^2}{2}\frac{f_{etu}-f_{etc}}{\varepsilon_{\text{etu}}-\varepsilon_{\text{etc}}}(\frac{2h_e\varepsilon_{\text{et}}}{3h_t}-\varepsilon_{\text{et}}+\varepsilon_{\text{etc}})-f_{sy}A_s h_s$	(29)

4 Cracking, yielding and ultimate moments of composite beams

4.1 Cracking moment

(1) Case 1: ECC cracking before concrete

When ECC incurs crack before concrete, $\varepsilon_{\text{et}}=\varepsilon_{\text{etc}}$, the neutral axis depth h_{t} can be obtained from Eq. (12), and the cracking moment in this case can be expresses as below:

$$M_{cr}=\frac{f_c b\varepsilon_{\text{etc}}}{\varepsilon_{co}}\left(\frac{2h^3}{3h_t}-h^2+\frac{h_t^2}{3}\right)-\frac{f_c b\varepsilon_{\text{etc}}^2}{\varepsilon_{co}^2}\left(\frac{h^4}{4h_t^2}-\frac{2h^3}{3h_t}+\frac{h^2}{2}-\frac{h_t^2}{12}\right)-$$
$$f_{etc}bh_e^2\left(\frac{1}{2}-\frac{h_e}{3h_t}\right)-\frac{f_{ctu}b\varepsilon_{\text{etc}}}{\varepsilon_{ctu}}\left(\frac{h_t^2}{6}-\frac{h_e^2}{2}+\frac{h_e^3}{3h_t}\right)-\frac{h_t-h_s}{h_t}\varepsilon_{\text{etc}}E_sA_sh_s \quad (30)$$

(2) Case 2: concrete cracking before ECC

When concrete cracks before ECC, the maximum tensile strain of concrete $\varepsilon_{\text{ct}}=\varepsilon_{\text{ctu}}$ and the maximum tensile strain of ECC $\varepsilon_{\text{et}}=\varepsilon_{\text{ctu}}h_t/(h_t-h_e)<\varepsilon_{\text{etc}}$. Substituting ε_{et} into Eq. (12), the neutral axis depth h_t can be calculated and the cracking moment in this case can be expressed as below:

$$M_{cr}=\frac{f_c b\varepsilon_{ctu}}{\varepsilon_{co}(h_t-h_e)}\left(\frac{2h^3}{3}-h^2h_t+\frac{h_t^3}{3}\right)-\frac{f_c b\varepsilon_{ctu}^2}{(h_t-h_e)^2\varepsilon_{co}^2}\left(\frac{h^4}{4}-\frac{2h^3h_t}{3}+\frac{h^2h_t^2}{2}-\frac{h_t^4}{12}\right)$$
$$-\frac{f_{etc}b\varepsilon_{ctu}}{\varepsilon_{etc}(h_t-h_e)}\left(\frac{h_e^2h_t}{2}-\frac{h_e^3}{3}\right)-\frac{f_{ctu}b}{h_t-h_e}\left(\frac{h_t^3}{6}-\frac{h_e^2h_t}{2}+\frac{h_e^3}{3}\right)-\frac{h_t-h_s}{h_t-h_e}\varepsilon_{ctu}E_sA_sh_s \quad (31)$$

4.2 Yield moment

(1) Case 1: Compressive concrete in the elastic stage after cracking

In such case, the maximum compressive strain in concrete $\varepsilon_c\le\varepsilon_{co}$, the tensile strain in steel bars $\varepsilon_s=\varepsilon_{sy}$ and the maximum tensile strain in ECC $\varepsilon_{et}=\varepsilon_{sy}h_t/(h_t-h_s)$, the neutral axis depth h_t can be calculated from Eq. (21) and the yield moment in this case can be expressed as below:

$$M_y=\frac{f_c b\varepsilon_{sy}}{\varepsilon_{co}(h_t-h_s)}\left(\frac{2h^3}{3}-h^2h_t+\frac{h_t^3}{3}\right)-\frac{f_c b\varepsilon_{sy}^2}{(h_t-h_s)^2\varepsilon_{co}^2}\left(\frac{h^4}{4}-\frac{2h^3h_t}{3}+\frac{h^2h_t^2}{2}\right.$$
$$\left.-\frac{h_t^4}{12}\right)-\frac{f_{etc}bh_e^2}{2}-\frac{bh_e^2}{2}\frac{f_{etu}-f_{etc}}{\varepsilon_{\text{etu}}-\varepsilon_{\text{etc}}}\left(\frac{h_t\varepsilon_{sy}}{h_t-h_s}-\varepsilon_{\text{etc}}-\frac{2h_e\varepsilon_{sy}}{3(h_t-h_s)}\right)-f_{sy}A_sh_s \quad (32)$$

(2) Case 2: Compressive concrete in the plastic stage after cracking

For this case, the maximum compressive strain of concrete $\varepsilon_{co}<\varepsilon_c\le\varepsilon_{cu}$, the tensile strain in steel bars $\varepsilon_s=\varepsilon_{sy}$ and the maximum tensile strain in ECC $\varepsilon_{et}=\varepsilon_{sy}h_t/(h_t-h_s)$. Substituting ε_{et} into Eq. (23), h_t can be calculated and the yield moment in this case can be expressed as below:

$$M_y=\frac{f_cbh^2}{2}-f_cb\left(\frac{(h_t-h_s)^2\varepsilon_{co}^2}{12\varepsilon_{sy}^2}+\frac{h_t^2}{2}+\frac{(h_t-h_s)h_t\varepsilon_{co}}{3\varepsilon_{sy}}\right)-\frac{f_{etc}bh_e^2}{2}$$
$$+\frac{bh_e^2}{2}\frac{f_{etu}-f_{etc}}{\varepsilon_{\text{etu}}-\varepsilon_{\text{etc}}}\left(\frac{2h_e\varepsilon_{sy}}{3(h_t-h_s)}-\frac{h_t\varepsilon_{sy}}{h_t-h_s}+\varepsilon_{\text{etc}}\right)-f_{sy}A_sh_s \quad (33)$$

4.3 Ultimate moment

(1) Case 1: Under-reinforced failure

The maximum compressive strain in concrete $\varepsilon_c=\varepsilon_{cu}$, the maximum compressive stress in concrete $\sigma_c=f_c$ and the maximum tensile strain in ECC $\varepsilon_{et}=\varepsilon_{cu}h_t/(h-h_t)$. Substituting ε_{et} into Eq. (28), h_t can be calculated and the ultimate moment in this case can be expressed as below:

$$M_u = \frac{f_c b h^2}{2} - f_c b\left(\frac{(h-h_t)^2\varepsilon_{co}^2}{12\varepsilon_{cu}^2} + \frac{h_t^2}{2} + \frac{(h-h_t)h_t\varepsilon_{co}}{3\varepsilon_{cu}}\right) - \frac{f_{etc} b h_e^2}{2} + \frac{b h_e^2}{2}\frac{f_{etu}-f_{etc}}{\varepsilon_{etu}-\varepsilon_{etc}}\left(\frac{2h_e\varepsilon_{cu}}{3(h-h_t)} - \frac{h_t\varepsilon_{cu}}{h-h_t} + \varepsilon_{etc}\right) - f_{sy}A_s h_s \quad (34)$$

(2) Case 2: Over-reinforced failure

If the composite beam is over-reinforced, steel reinforcement would not yield while compressive strain in concrete reaches the ultimate crushing strain. In this case, $\varepsilon_c = \varepsilon_{cu}$ and $\varepsilon_s < \varepsilon_{sy}$, the maximum tensile strain in ECC, ε_{et}, and strain in steel reinforcement, ε_s, can be obtained according to the geometrical relationship, $\varepsilon_{et} = \varepsilon_{cu}h_t/(h-h_t)$, $\varepsilon_s = \varepsilon_{cu}(h_t-h_s)/(h-h_t)$. The neutral axis depth h_t can be calculated by Eq. (26) and the ultimate moment of this case can be expressed as below:

$$M_u = \frac{f_c b h^2}{2} - f_c b\left(\frac{(h-h_t)^2\varepsilon_{co}^2}{12\varepsilon_{cu}^2} + \frac{h_t^2}{2} + \frac{(h-h_t)h_t\varepsilon_{co}}{3\varepsilon_{cu}}\right) - \frac{f_{etc} b h_e^2}{2} + \frac{b h_e^2}{2}\frac{f_{etu}-f_{etc}}{\varepsilon_{etu}-\varepsilon_{etc}}\left(\frac{2h_e\varepsilon_{cu}}{3(h-h_t)} - \frac{h_t\varepsilon_{cu}}{h-h_t} + \varepsilon_{etc}\right) - \frac{h_t-h_s}{h-h_t}\varepsilon_{cu}E_s A_s h_s \quad (35)$$

(3) Case 3: Steel-reinforcement rupture failure

When the area of steel reinforcement is too small to allow steel bars rupture before compressive concrete reaches the plastic stage. In this case, $\varepsilon_c < \varepsilon_{co}$ and $\varepsilon_s = \varepsilon_{su}$, the maximum tensile strain in ECC ε_{et} and the maximum compressive strain in concrete ε_c can be obtained according to the geometrical relationship of cross-section, $\varepsilon_{et} = \varepsilon_{su}h_t/(h_t-h_s)$, $\varepsilon_c = \varepsilon_{su}(h-h_t)/(h_t-h_s)$. The neutral axis depth h_t can be calculated by Eq. (23) and the ultimate moment of this case can be expressed as below:

$$M_u = \frac{f_c b\varepsilon_{su}}{\varepsilon_{co}(h_t-h_s)}\left(\frac{2h^3}{3} - h^2h_t + \frac{h_t^3}{3}\right) - \frac{f_c b\varepsilon_{su}^2}{(h_t-h_s)^2\varepsilon_{co}^2}\left(\frac{h^4}{4} - \frac{2h^3h_t}{3} + \frac{h^2h_t^2}{2} - \frac{h_t^4}{12}\right) - \frac{f_{etc} b h_e^2}{2} - \frac{b h_e^2}{2}\frac{f_{etu}-f_{etc}}{\varepsilon_{etu}-\varepsilon_{etc}}\left(\frac{h_t\varepsilon_{su}}{h_t-h_s} - \varepsilon_{etc} - \frac{2h_e\varepsilon_{su}}{3(h_t-h_s)}\right) - f_{sy}A_s h_s \quad (36)$$

It is to be noted that it is unlikely that ECC reaches the ultimate tensile strain before yielding steel due to the high tensile strain ε_{etu} of ECC at failure; therefore, this mode of failure is not considered.

4.4 Deflection

The curvature of a composite beam is shown in figure 5, where ρ is the curvature radius of deformed composite beam, $d\theta$ is the rotating angle increment of cross-section. The maximum tensile strain in ECC ε_{et} can be calculated as below:

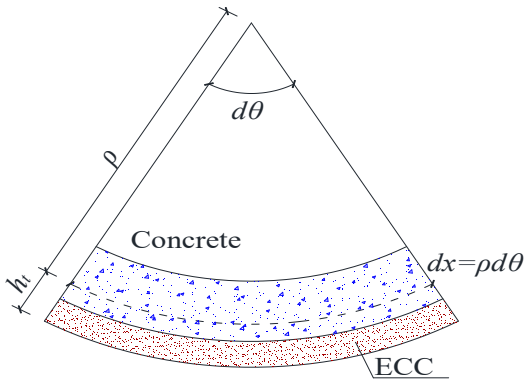

Fig.5 Curvature distribution of composite beam unit

$$\varepsilon_{\mathrm{et}} = \frac{(\rho + h_t)d\theta - \rho d\theta}{\rho d\theta} = h_t / \rho \tag{37}$$

The cross-section curvature of a composite beam can be also expressed as below:

$$\varphi = 1/\rho = \varepsilon_{\mathrm{et}} / h_t \tag{38}$$

Based on the above analysis, $\varepsilon_{\mathrm{et}}$ and h_{t} for different moments can be obtained. Substituting $\varepsilon_{\mathrm{et}}$, h_{t} into formula (38), the curvature at different moments can be calculated.

According to the theory of structural mechanics, the maximum deflection at mid-span of a simply supported beam can be calculated as below:

$$f = SMl_0^2 / (EI) \tag{39}$$

where f is the maximum deflection at mid-span, S is a coefficient related to loading and supporting condition, M is the moment acting on the cross-section, l_0 is the element length, E is the elastic modulus of sectional material and I is the inertia moment of cross-section. As the flexural stiffness of cross-section $EI = M/\varphi$, formula (39) can be expressed as below:

$$f = Sl_0^2 / \rho = Sl_0^2 \varepsilon_{\mathrm{et}} / h_t \tag{40}$$

4.5 Ductility and energy dissipation

The moment-curvature model of composite beams is shown in figure 6, where M_{cr} and φ_{cr} are the cracking moment and corresponding curvature, respectively, M_{y} and φ_{y} are the yield moment and corresponding curvature, respectively, M_{u} and φ_{u} are the ultimate moment and corresponding curvature, respectively.

The composite beam ductility can be calculated from $u_{\varphi} = \varphi_{\mathrm{u}}/\varphi_{\mathrm{y}}$, whereas the area under the M-φ curve is used to represent the energy dissipation capacity. In the elastic stage, the actual M-φ curve is the solid line and it is simplified to the dotted line as shown in the model in figure 6.

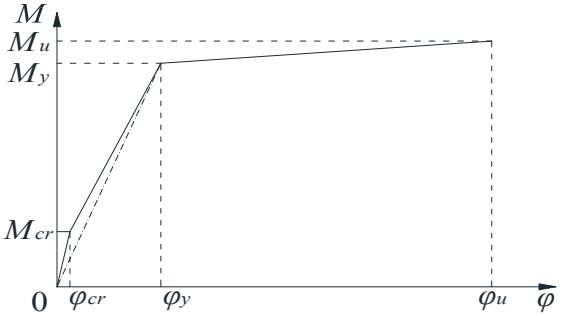

Fig.6 Moment-curvature of composite beams

Energy dissipation capacity of elastic stage can be calculated as below:

$$E_{\mathrm{y}} = M_{\mathrm{y}}\varphi_{\mathrm{y}}/2 \tag{41}$$

Energy dissipation capacity of the whole stage (up to φ_{u}) can be calculated as below:

$$E_{\mathrm{p}} = M_{\mathrm{y}}\varphi_{\mathrm{y}}/2 + (M_{\mathrm{y}}+M_{\mathrm{u}})(\varphi_{\mathrm{u}}-\varphi_{\mathrm{y}})/2 \tag{42}$$

In order to compare the energy dissipation capacity of the whole stage with the elastic stage, energy dissipation ratio r_{E} is introduced.

$$r_{\mathrm{E}} = E_{\mathrm{p}}/E_{\mathrm{y}} \tag{43}$$

5 Experimental verifications

In this section, physical testing results of composite ECC/concrete beams reinforced with steel bars are presented. The main purpose of the experimental programme is to provide real data for the validation of the proposed analytical procedure presented above before it is used for a comprehensive parametric study.

5.1 Test specimens design

Three group specimens with different strength of steel reinforcement were cast and tested [36]. Each group had four specimens with different ECC thickness whereas the grade of main longitudinal steel was the main parameter changed from one group to another. Design details are shown in table 2 and the schematic diagram of specimens is shown in figure 7. The specimen size $b \times h \times l$ = 150 × 200 × 1500 mm, pure flexural span l_m = 400 mm, flexural-shear span l_{mv} = 500 mm, free overhang span l_f = 50 mm, cross-section effective height h_0 = 175 mm, distance of the center of steel bars to concrete tensile edge h_s = 25mm, h_e is the thickness of ECC, r_h is ECC height replacement ratio, defined as the ratio of ECC thickness to the height of the beam cross-section, $r_h = h_e / h_0$. All notations are defined in figure 7. In casting ECC-concrete composite test specimens, the layered pouring method was adopted, where ECC was poured into the mould first and compacted, and then concrete was poured and compacted. This technique proved to achieve a good bond between ECC and concrete [35].

Table 2 Specimen design parameters

NO.	longitudinal steel reinforcement	stirrup	erection bars	height replacement ratio r_h
CBSA	2Φ12	Φ8@125	2Φ10	0.00/0.29/0.57/1.14
CBSE	2Φ12	Φ8@100	2Φ10	0.00/0.29/0.57/1.14
CBSF	2Φ12	Φ8@100	2Φ10	0.00/0.57/1.14

Note: Φ, HRB335 steel bar; Φ, HRB400 steel bar; Φ, HRB500 steel bar.

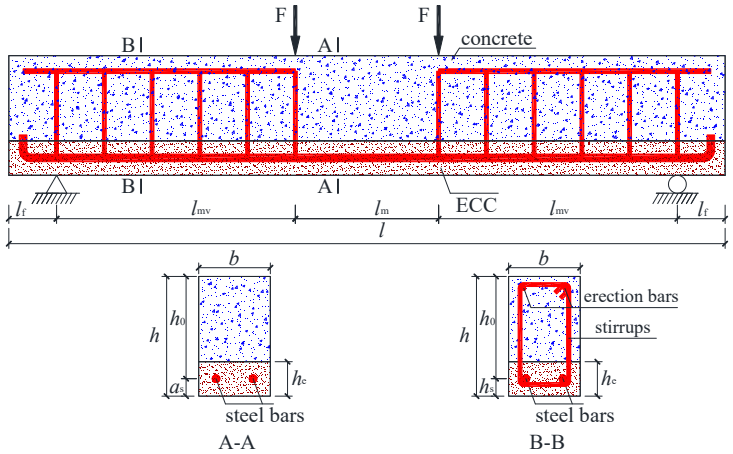

Fig.7 Schematic diagram of ECC-concrete composite beams

5.2 Materials

The concrete mechanical properties as required by the model presented in figure 2 were measured [37]: the cube compressive strength $f_{cu,k}$ = 47.00 N·mm^{-2}, compressive strength f_c = 30.16 N·mm^{-2}, tensile strength f_{ct} = 2.55 N·mm^{-2} and ultimate tensile strain $\varepsilon_{ctu} = 1.10\times10^{-4}$. On the other hand, mechanical properties of steel reinforcement [38] are shown in table 3.

Table 3 Mechanical properties of steel reinforcement

Bars	Diameter / mm	f_{sy} / (N·mm^{-2})	f_{su} / (N·mm^{-2})	E_s / (1×10^3 N·mm^{-2})

HRB335	12	340	460	199
HRB400	8	406	485	198
HRB400	10	403	495	198
HRB400	12	408	503	199
HRB500	12	507	630	199

Tensile and compressive tests of ECC were also conducted [39], and multiple cracks and tensile stress-strain curves are shown in figure 8(a) and 8(b), respectively. The tensile strength at first cracking f_{etc} = 2.0 N·mm^{-2}, ultimate tensile strength f_{etu} = 2.4 N·mm^{-2}, tensile strain at first cracking $\varepsilon_{etc} = 0.23\times10^{-3}$, ultimate tensile strain ε_{etu} = 0.025, compressive strength f_{ecp} = 31.4 N·mm^{-2} and corresponding strain ε_{ecp} = 0.0036. The compressive stress-strain curves of ECC are also shown in figure 9.

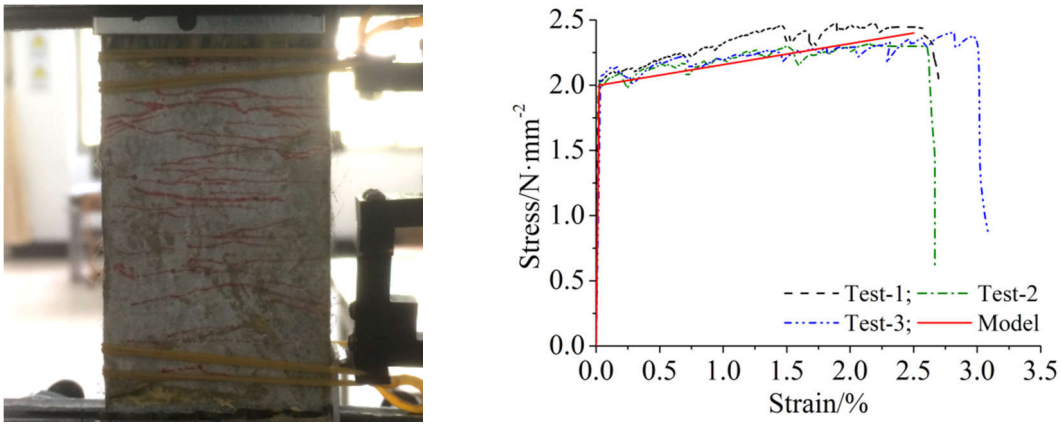

(a) Multiple cracks (b) Stress-strain curves

Fig.8 Typical characteristics of ECC in tension

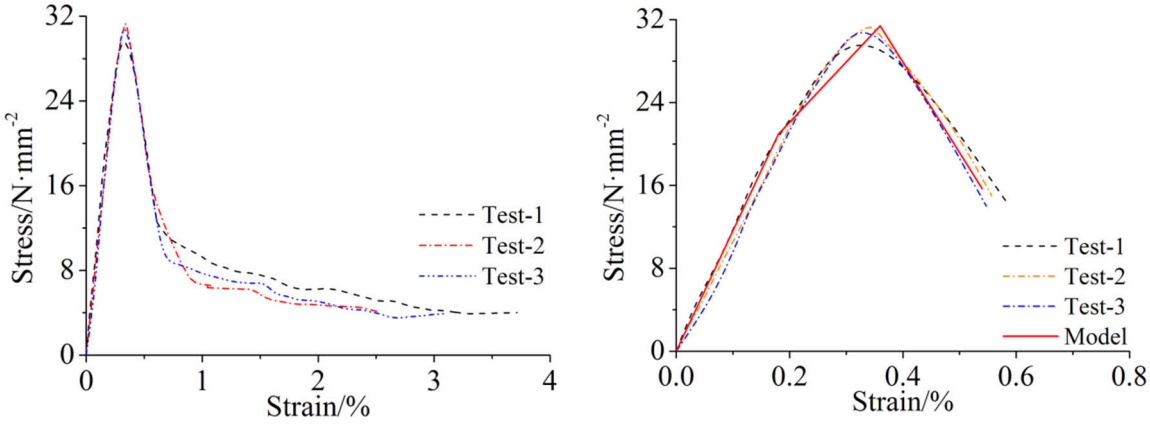

(a) Whole curves (b) Local curves and fitting curve

Fig.9 Compressive stress-strain curves of ECC

5.3 Comparison between experimental and theoretical results

Comparisons of experimental and calculated load-deflection curves are shown in figure 10 for specimens of group CBSE. As can be seen from this figure, experimental and predicted curves show good agreements. The predicted ultimate moment is always lower than the experimental moment as the yield strength of steel reinforcement is used in the calculation instead of ultimate tensile strength. Comparisons of cracking, yield and ultimate moments are also presented in table 4, where $M_{cr,t}$, $M_{y,t}$ and $M_{u,t}$ are experimental cracking, yield and ultimate moment, respectively, $M_{cr,c}$ and $M_{y,c}$ are predicted cracking and yield moment, respectively, $M_{u,c1}$ and $M_{u,c2}$ are calculated ultimate moment by using yield strength and ultimate strength of steel reinforcement, respectively.

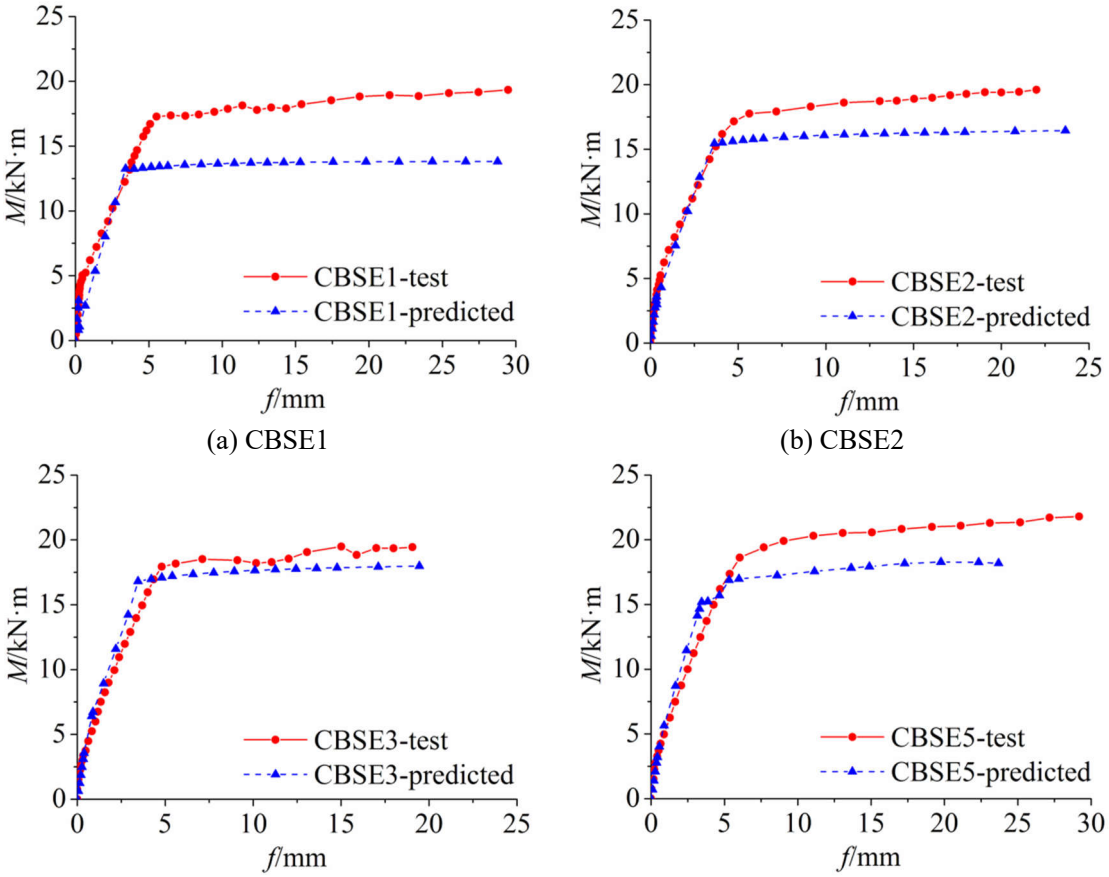

(a) CBSE1 (b) CBSE2

(c) CBSE3 (d) CBSE5

Fig.10 Comparison of moment-deflection curves

Table 4 Comparison of cracking, yield, ultimate moment (unit / kN·m)

NO.	r_h	$M_{cr,e}$	$M_{y,e}$	$M_{u,e}$	$M_{cr,c}$	$M_{y,c}$	$M_{u,c1}$	$M_{u,c2}$	$M_{cr,c}/M_{cr,e}$	$M_{y,c}/M_{y,e}$	$M_{u,c1}/M_{u,e}$	$M_{u,c2}/M_{u,e}$
CBSA1	0.00	3.00	11.30	16.78	3.08	10.67	11.64	15.47	1.03	0.94	0.69	0.92
CBSA2	0.29	4.06	14.00	18.75	3.60	13.37	14.41	18.05	0.89	0.96	0.77	0.96
CBSA3	0.57	3.99	15.78	19.35	3.57	14.75	16.04	19.58	0.89	0.93	0.83	1.01
CBSA5	1.14	3.48	15.05	19.37	3.20	14.67	16.33	19.53	0.92	0.98	0.84	1.01
CBSE1	0.00	3.26	14.69	19.25	3.08	13.26	13.83	16.82	0.94	0.90	0.72	0.87
CBSE2	0.29	3.74	16.18	19.50	3.60	15.46	16.48	19.33	0.96	0.96	0.85	0.99
CBSE3	0.57	3.75	17.93	19.75	3.57	16.82	18.05	20.83	0.95	0.94	0.91	1.05
CBSE5	1.14	3.26	17.36	22.50	3.20	15.71	18.19	20.68	0.98	0.90	0.81	0.92
CBSF1	0.00	3.28	16.95	21.04	3.08	15.88	16.72	20.68	0.94	0.94	0.79	0.98
CBSF3	0.57	3.71	20.69	23.26	3.57	19.89	20.74	24.43	0.96	0.96	0.89	1.05
CBSF5	1.14	3.74	17.69	22.60	3.20	17.93	20.60	23.88	0.86	1.01	0.91	1.06
							mean		0.94	0.94	0.82	0.99
							variation		0.05	0.06	0.09	0.06

As can be seen from table 4, average values of $M_{cr,c}$ / $M_{cr,e}$, $M_{y,c}$ / $M_{y,e}$, $M_{u,c1}$ / $M_{u,e}$ and $M_{u,c2}$ / $M_{u,e}$ are 0.94, 0.94, 0.82 and 0.99, respectively, and their variation coefficients are 0.05, 0.06, 0.09 and 0.06, respectively, showing good agreement between predicted and experimental moment results.

Loading-deflection curves and loading-crack width curves of group CBSE are shown in figure 11 and figure 12, respectively.

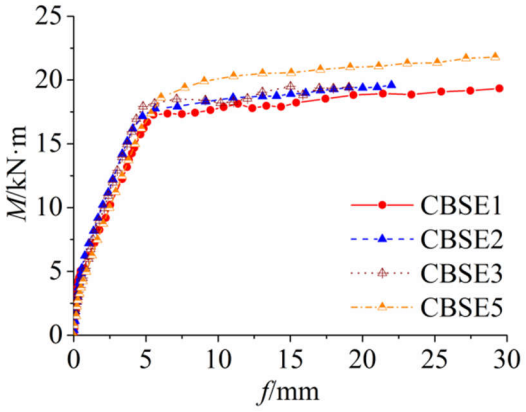

Fig.11 Loading-deflection curves

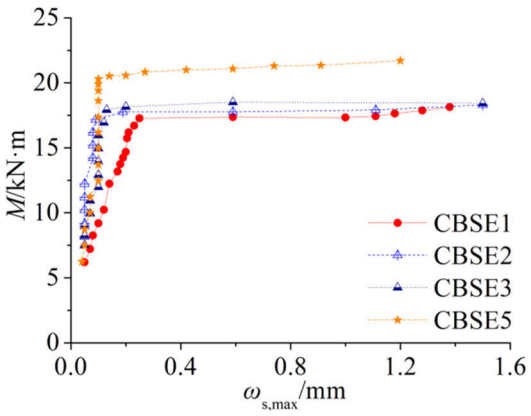

Fig.12 Loading-crack width curves

As can be seen from table 4, figure 11 and figure 12, compared with normal concrete beam (CBSE1), ECC-concrete composite beams (CBSE2, CBSE3) and ECC beam (CBSE5) are slightly improved both the flexural capacity and deformation ability, but significantly reduced the crack width before yielding of steel reinforcement.

6 Parametric studies

In this section, the effect of main parameters, such as ECC height replacement ratio, reinforcement ratio, strength of steel reinforcement, concrete and ECC on mechanical behaviors of composite beams are examined. When one parameter is changed, other basic parameters are kept constant at the following values: ECC height replacement ratio r_h is 0.29, reinforcement ratio ρ_s are 0.6% and 1.53%, yield strength of steel reinforcement f_{yk} is 400 N·mm^{-2}, compressive strength of C45 grade concrete f_c is 29.6 N·mm^{-2}, ECC tensile strength at first cracking f_{etc} is 2.0 N·mm^{-2}, ECC ultimate tensile strength f_{tu} is 2.4 N·mm^{-2}, ECC tensile strain at first cracking ε_{etc} is 0.00025 and ECC ultimate tensile strain ε_{etu} is 0.025.

The composite beam cross-section is assumed to be failed when maximum concrete compressive strain, ε_c, tensile strains in steel bars, ε_s, or tensile strains in ECC, ε_{et}, reaches 0.0033, 0.01 or 0.025, respectively. The failure modes can be predicted by the proposed model, namely tensile failure (tensile strain in steel reinforcement reaches ε_{su} first), compressive failure (concrete compressive strain reaches ε_{cu} after yielding of steel reinforcement) and over-reinforced failure (concrete compressive strain reaches ε_{cu} before yielding of steel reinforcement). In order to distinguish the three failure modes, two balanced failure points are identified, namely balanced failure point 1 is defined when tensile strain in steel reinforcement and maximum concrete compressive strain simultaneously reaches their respective ultimate values, whereas balanced failure point 2 indicates tensile strain in steel reinforcement reaches yield strain and maximum concrete compressive strain reach the ultimate strain at the same time. The ultimate values of each material are defined above.

6.1 ECC Strength and height replacement ratio

The correlation curves of mechanical behavior and the ECC Strength f_{etu}, ECC height replacement ratio r_h are shown in figure 13. Two steel reinforcement ratios ρ_s (0.60% and 1.53%), five height replacement ratios r_h (0, 0.14, 0.29, 0.43 and 0.57) and eight ECC strengths (f_{etc1} = 1.5 N·mm^{-2}, f_{etu1} = 1.8N·mm^{-2}, f_{etc2} = 2.0 N·mm^{-2}, f_{etu2} = 2.4N·mm^{-2}, f_{etc3} = 2.5 N·mm^{-2}, f_{etu3} = 3.0N·mm^{-2}, f_{etc4} = 3.0 N·mm^{-2}, f_{etu4} = 3.6N·mm^{-2}, f_{etc5} = 3.5 N·mm^{-2}, f_{etu5} = 4.2N·mm^{-2}, f_{etc6} = 4.0 N·mm^{-2}, f_{etu6} = 4.8N·mm^{-2}, f_{etc7} = 4.5

N·mm^{-2}, f_{etu7} = 5.4N·mm^{-2}, f_{etc8} = 5.0 N·mm^{-2}, f_{etu8} = 6.0N·mm^{-2}) are studied.

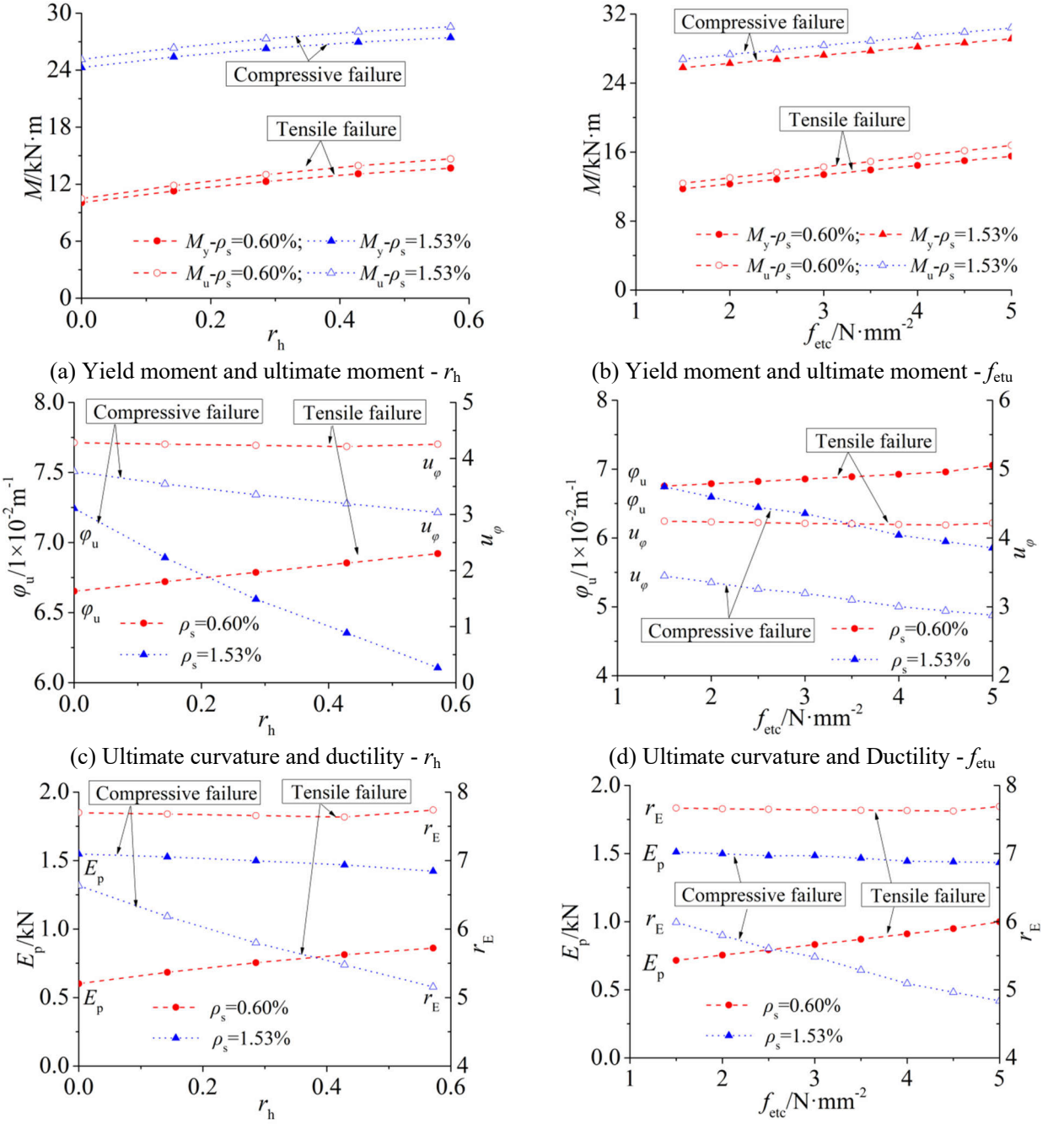

(a) Yield moment and ultimate moment - r_h

(b) Yield moment and ultimate moment - f_{etu}

(c) Ultimate curvature and ductility - r_h

(d) Ultimate curvature and Ductility - f_{etu}

(e) Energy disspation and energy dissipation ratio - r_h

(f) Energy dissipation and energy dissipation ratio - f_{etu}

Fig.13 Effect of ECC Strength and height replacement ratio

As can be seen from Fig. 13, the yield and ultimate moments increase with increasing the strength or the height replacement ratio of ECC; the moment increasing rate of beams with lower reinforcement ratio (ρ_s = 0.6%) is higher than that of beams with higher reinforcement ratio (ρ_s = 1.53%).

For composite beams with lower reinforcement ratio (ρ_s = 0.6%), failure modes are tensile failure - rupture of steel reinforcement. With increasing the ECC strength or the ECC height replacement ratio, ECC can provide more tensile resistance. In order to provide more compression to counterpoise the increased tensile resistance, maximum concrete compressive strain increases accordingly. So, the ultimate curvature increases as maximum concrete compressive strain increases while the tensile rupture strain of steel reinforcement is a fixed value.

For composite beams with higher reinforcement ratio (ρ_s = 1.53%), failure modes are compressive failure - crushing of concrete. With increasing the ECC strength or the ECC height replacement ratio, ECC can provide more tensile resistance. The tensile resistance provided by ECC together with less tensile resistance (compared with the specimen with lower ECC strength or lower ECC height replacement ratio) provided by steel reinforcement can counterpoise concrete compression, then maximum tensile strain of steel reinforcement decreases accordingly. So, the ultimate curvature decreases as the strain of steel reinforcement decreases while the ultimate concrete crushing compressive strain is a fixed value.

For composite beams with lower reinforcement ratio (ρ_s = 0.6%), yield moment, yield curvature, ultimate moment and ultimate curvature increase with increasing the ECC strength or the ECC height replacement ratio. So, ductility and energy dissipation ratio essentially unchanging, but the energy dissipation gradually increases. For composite beams with higher reinforcement ratio (ρ_s = 1.53%), yield moment, yield curvature and ultimate moment increase while ultimate curvature significantly decreases with increasing the ECC strength or the ECC height replacement ratio. So, ductility, energy dissipation and energy dissipation ratio gradually decrease.

6.2 Amount of steel reinforcement

The correlation curves of mechanical behavior and reinforcement ratio ρ_s are shown in figure 14. Ten reinforcement ratios ρ_s (0.19%, 0.38%, 0.60%, 0.86%, 1.03%, 1.20%, 1.36%, 1.63%, 1.83% and 1.96%) and two tensile strengths of ECC (f_{etc1} = 2.0 N·mm^{-2}, f_{etu1} = 2.4 N·mm^{-2}, f_{etc2} = 4.0 N·mm^{-2} and f_{etu2} = 4.8N·mm^{-2}) are studied. The notation used in figure 12 is explained below: ECC-2.0-A indicates a composite beam with ECC tensile strength f_{etc} = 2.0 N·mm^{-2} and A indicates incur tensile failure, B indicates incur compressive failure and C indicates incur over-reinforced failure.

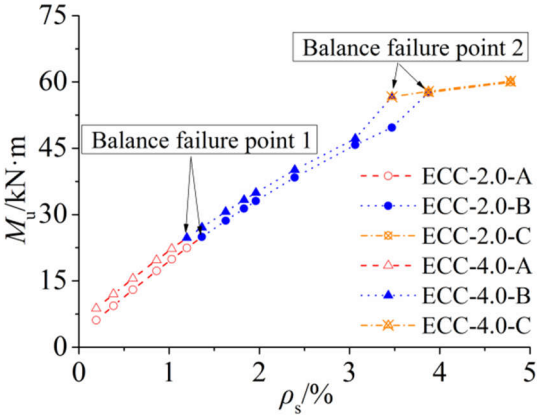

(a) Ultimate moment

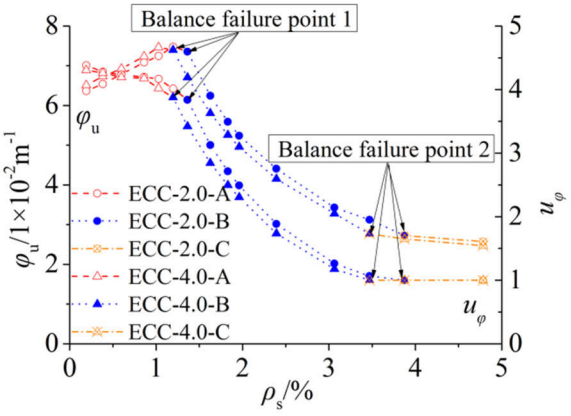

(b) Ultimate curvature and Ductility

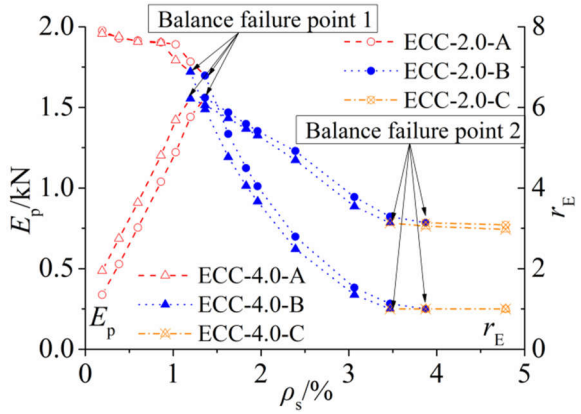

(c) Energy dissipation and energy dissipation ratio

Fig.14 Effect of reinforcement ratio

As can be seen from Fig. 14, the ultimate moment increases with increasing the reinforcement ratio; however, the increasing rate before balanced failure point 2 is much higher than that after balanced failure point 2. As ECC-4.0 can provide more tensile resistance than ECC-2.0, the reinforcement ratio of balanced failure point 1 and point 2 of ECC-4.0 are lower than that of ECC-2.0.

With increasing the reinforcement ratio, the ultimate curvature gradually increases before balanced failure point 1, significantly decreases before balanced failure point 2, and then smoothly decreases after point 2. For tensile failure stage, the tensile rapture strain of steel reinforcement is a fixed value. With increasing the reinforcement ratio, steel reinforcement can provide more tensile resistance, maximum concrete compressive strain increases and, then, the ultimate curvature increases correspondingly. For compressive failure mode, ultimate concrete compressive crushing strain is a fixed value. With increasing the reinforcement ratio, lower tensile stress/strain of steel reinforcement can provide enough tensile resistance to counterpoise concrete compression, and then ultimate curvature decreases correspondingly.

Yield moment, yield curvature, ultimate moment and ultimate curvature increase with increasing the reinforcement ratio before balanced failure point 1, and the increase rate of ultimate curvature is lower than that of yield curvature. So, ductility and energy dissipation ratio gradually decrease, and energy dissipation gradually increases. Yield moment, yield curvature and ultimate moment increase but ultimate curvature decreases between balanced failure point 1 and point 2. So, ductility decreases faster, and energy dissipation and energy dissipation ratio gradually decrease.

6.3 Strength of steel reinforcement

The correlation curves of mechanical behavior and strength of steel reinforcement are shown in figure 15. Four standard yield strengths of steel reinforcement f_{yk} (300 N·mm^{-2}, 335 N·mm^{-2}, 400 N·mm^{-2} and 500 N·mm^{-2}) and two reinforcement ratios ρ_s (0.6% and 1.53%) are studied.

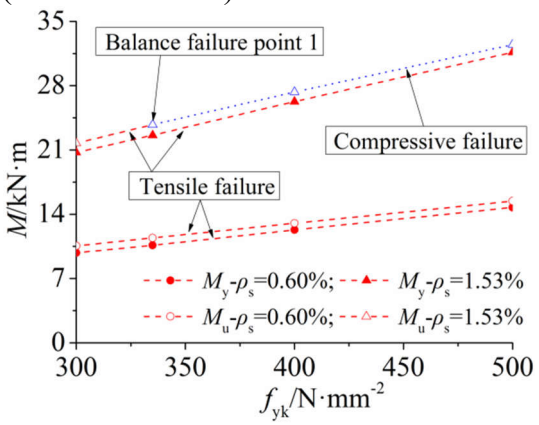

(a) Yield moment and ultimate moment

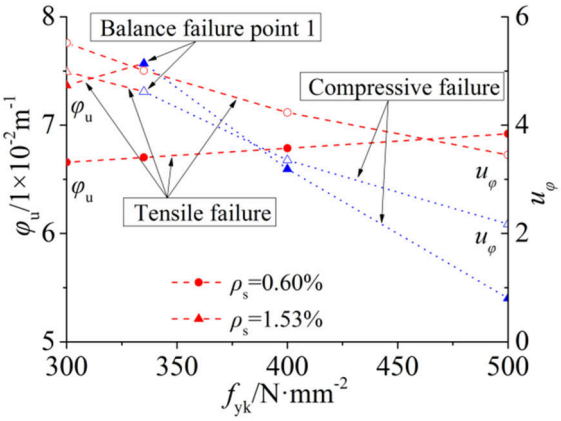

(b) Ultimate curvature and Ductility

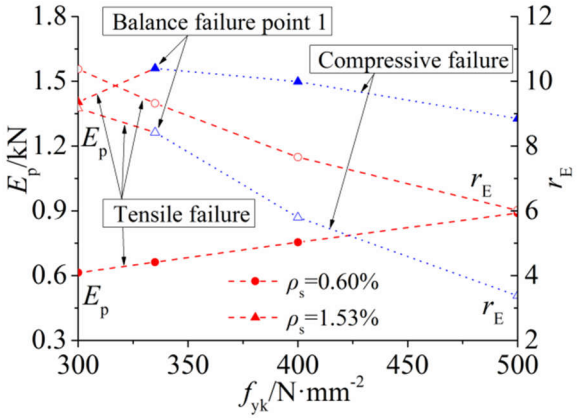

(c) Energy dissipation and energy dissipation ratio

Fig.15 Effect of strength of steel bars

As can be seen from Fig. 15, yield moment and ultimate moment increase with increasing the strength of steel reinforcement. Composite beams with lower reinforcement ratio (ρ_s = 0.6%) all incur tensile failure, whereas, composite beams with higher reinforcement ratio (ρ_s = 1.53%) incur tensile failure before balanced failure point 1 and then incur compressive failure.

For composite beams with lower reinforcement ratio (ρ_s = 0.6%), failure modes are tensile failure - rupture of steel reinforcement, the tensile rapture strain of steel reinforcement is a fixed value. With increasing the strength of steel reinforcement, steel reinforcement can provide more tensile resistance, maximum concrete compressive strain increases to provide more resistance to counterpoise the tension, and then ultimate curvature increases correspondingly. For composite beams with higher reinforcement ratio (ρ_s = 1.53%), ultimate curvature increases before point 1 and then decreases.

For composite beams with 0.6% reinforcement ratio, yield moment, yield curvature, ultimate moment and ultimate curvature increase with increasing the strength of steel reinforcement. However, the increase rate of ultimate curvature is lower than that of yield curvature. So, ductility and energy dissipation ratio gradually decrease but energy dissipation increases. For composite beams with 1.53% reinforcement ratio, the situation is the same as composite beams with 0.6% reinforcement ratio before balanced failure point 1. However, ultimate curvature decreases after point 1. So, energy dissipation and energy dissipation ratio decrease and ductility decreases faster.

6.4 Concrete strength

The correlation curves of mechanical behavior and concrete strength are shown in figure 16. Eight concrete grades (C25, C30, C35, C40, C45, C50, C55 and C60) and two reinforcement ratios ρ_s (0.6% and 1.53%) are studied.

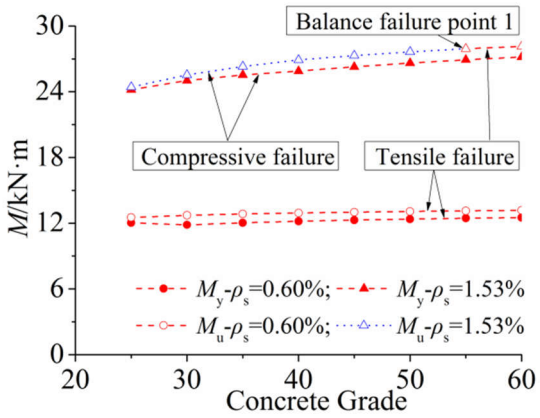

(a) Yield moment and ultimate moment

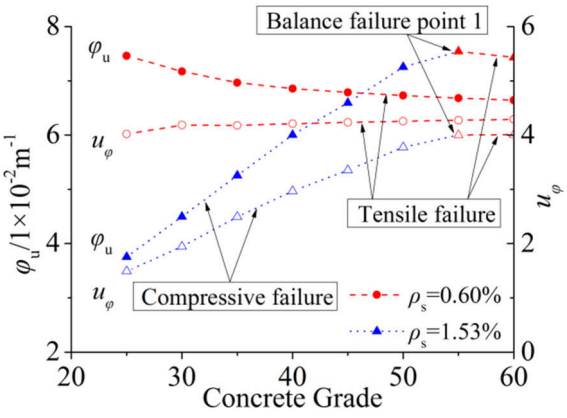

(b) Ultimate curvature and Ductility

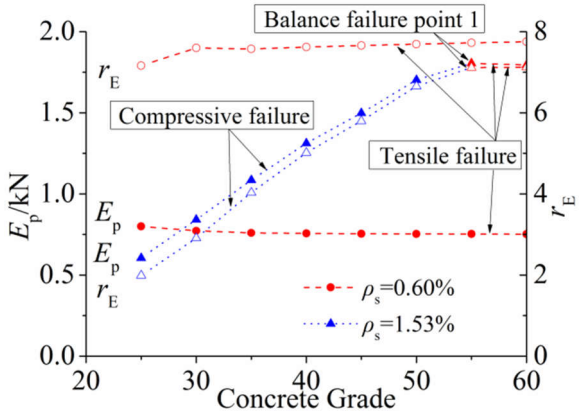

(c) Energy dissipation and energy dissipation ratio

Fig.16 Effect of concrete strength

As can be seen from Fig. 16, yield and ultimate moment increase with increasing the concrete strength, and the increasing rate of beams with higher reinforcement ratio (ρ_s = 1.53%) are higher than that of beams with lower reinforcement ratio (ρ_s = 0.6%) due to the failure mode in each case, tensile and compressive failure, respectively. In case of tensile rupture of steel reinforcement, increasing the concrete strength is not as effective as the compressive failure of concrete.

For composite beams with 0.6% reinforcement ratio, failure modes are tensile failure - rapture of steel reinforcement. With increasing concrete strength, lower concrete compressive stress/strain can provide enough compression to counterpoise the tensile resistance, and then ultimate curvature decreases correspondingly.

For composite beams with 1.53% reinforcement ratio, failure modes before point 1 are compressive failure - crushing of concrete. With increasing the concrete strength, concrete can provide more resistance, tensile stress/strains of steel reinforcement increase to counterpoise concrete compression, and then ultimate curvature increase correspondingly. Failure modes after point 1 are tensile failure, then ultimate curvature decrease.

For composite beams with 0.6% reinforcement ratio, yield and ultimate moment increase while yield curvature and ultimate curvature decrease with increasing the concrete strength. However, the decreasing rate of ultimate curvature is lower than that of yield curvature. Therefore, ductility gradually increases, energy dissipation and energy dissipation ratio essentially unchanged. On the other hand, for composite beams with 1.53% reinforcement ratio, yield and ultimate moment increase while yield curvature decreases with increasing the strength of concrete, ultimate curvature

increases before balanced failure point 1 and then decreases. So, ductility, energy dissipation and energy dissipation ratio gradually increase before point 1 and then essentially unchanged.

7 Conclusions

Mechanical behavior of composite beams is analysed and parametric analysis is conducted. The following conclusions are obtained:

(1) Based on the simplified constitutive models of materials and equilibrium of internal forces and moment, formulas for cracking, yield and ultimate moment as well as deflection are derived. Good agreement between the predicted and experimental results was obtained, confirming the applicability of the proposed formulas for use in practice.

(2) Yield moment and ultimate moments increase with increasing the tensile resistance, for example by increasing ECC height replacement ratio, reinforcement ratio, strength of steel reinforcement and ECC. However, with increasing the concrete compressive strength, yield and ultimate moments increase in case of compressive failure, but essentially unchanged in case of tensile failure.

(3) With increasing the tensile resistance, for example by increasing ECC height replacement ratio, reinforcement ratio, strength of steel reinforcement and ECC, ultimate curvature increases in case of tensile failure and decreases in case of compressive failure. With increasing the concrete strength, ultimate curvature decreases in case of tensile failure but increases in case of compressive failure. Ultimate curvature essentially unchanged in case of over-reinforced beams.

(4) In case of compressive failure, ductility decreases with increasing the tensile resistance, for example by increasing ECC height replacement ratio, reinforcement ratio, strength of steel reinforcement and ECC, but increases with increasing the concrete strength. On the other hand, in case of tensile failure, ductility essentially unchanged with increasing the ECC height replacement ratio and the ECC strength, gradually decreases with increasing the reinforcement ratio and the strength of steel reinforcement, but increases with increasing the concrete strength. Ductility essentially unchanged for over-reinforced beams.

(5) With increasing the tensile resistance, for example by increasing ECC height replacement ratio, reinforcement ratio, strength of steel reinforcement and ECC, energy dissipation increases in case of tensile failure but decreases in case of compressive failure. With increasing the concrete strength, energy dissipation essentially unchanged in case of tensile failure but increases in case of compressive failure. Energy dissipation essentially unchanged for over-reinforced beams.

(6) Energy dissipation ratio decreases with increasing the tensile resistance, for example by increasing reinforcement ratio and strength of steel reinforcement, but essentially unchanged with increasing the ECC height replacement ratio and the ECC strength in case of tensile failure. With increasing the concrete strength, energy dissipation ratio essentially unchanged in case of tensile failure but increase in case of compressive failure. Energy dissipation ratio essentially unchanged for over-reinforced beams.

Acknowledgement

The authors appreciate the support of the National Natural Science Foundation of China (51678514, 51308490), the Natural Science Foundation of Jiangsu Province, China (BK20130450), Six Talent Peaks Project of Jiangsu Province (JZ-038, 2016), Graduate Practice Innovation Project of Jiangsu Province (SJCX17-0625) and the Jiangsu Government Scholarship for Overseas Studies.

Notation

The following symbols are used in this paper:

ε_s = tensile strain in steel bar;
σ_s = tensile stress in steel bar;
f_{sy} = yield strength of steel bar;
ε_{sy} = yield strain of steel bar;
E_s = elastic modulus of steel bar;
ε_{su} = ultimate tensile strain of steel bar;
ε_c = compressive strain in concrete;
σ_c = compressive stress in concrete;
f_c = concrete compressive strength;
ε_{co} = compressive strain corresponding to concrete stress of f_c;
ε_{cu} = ultimate compressive strain of concrete;
$f_{cu,k}$ = concrete cube compressive strength;
n = a coefficient related to the compressive stress-strain relationship of concrete;
ε_{ct} = tensile strain in concrete;
σ_{ct} = tensile stress in concrete;
ε_{ctu} = ultimate uniaxial tensile strain of concrete;
f_{ctu} = ultimate uniaxial tensile stress of concrete;
ε_{ec} = compressive strain in ECC;
σ_{ec} = compressive tress in ECC;
f_{ecp} = compressive strength of ECC (peak point of ECC compressive stress-strain curve);
ε_{ecp} = compressive strain corresponding to peak stress of ECC f_{ecp};
f_{ecu} = ultimate compressive stress of ECC (after peak point);
ε_{ecu} = ultimate compressive strain corresponding to ultimate stress of ECC f_{ecu};
ε_{et} = tensile strain in ECC;
σ_{et} = tensile stress in ECC;
f_{etc} = tensile stress of ECC at first cracking;
ε_{etc} = tensile strain of ECC at first cracking;
f_{etu} = ultimate tensile strength of ECC;
ε_{etu} = ultimate tensile strain of ECC;
b = width of cross-section;
h = height of cross-section;
h_s = distance of the center of steel bars to the cross-section tensile edge;
h_e = thickness of ECC;
h_t = height of cross-section part in tension (neutral axis depth);
x = vertical distance of any point to the tensile edge of cross-section;
h_p = vertical distance of concrete where its strain reaches ε_{co} to the tensile edge of

cross-section;

ρ = curvature radius of deformed composite beam;

$d\theta$ = rotating angle increment of cross-section;

φ = curvature of deformed composite beam;

f = maximum deflection of specimen at mid-span;

S = a coefficient related to loading and supporting condition;

M = moment acting on the cross-section;

l_0 = length of composite beam;

E = elastic modulus of sectional material;

I = inertia moment of cross-section;

M_{cr} = cracking moment of cross-section;

φ_{cr} = cross-section curvature corresponding to cracking moment;

M_y = yield moment of cross-section;

φ_y = cross-section curvature corresponding to yield moment;

M_u = ultimate moment of cross-section;

φ_u = cross-section curvature corresponding to ultimate moment;

u_φ= curvature ductility of cross-section;

E_y = energy dissipation capacity of elastic stage;

E_p = energy dissipation capacity of whole stage (up to ultimate curvature φ_u);

r_E = energy dissipation ratio;

l = length of composite beam;

l_m = length of the pure flexural span;

l_{mv} = length of the flexural-shear span;

l_f = length of the free overhang span;

r_h = ECC height replacement ratio;

h_0 = effective height of cross-section;

f_{su} = ultimate tensile strength of steel bar;

$M_{cr,t}$ = experimental cracking moment;

$M_{y,t}$ = experimental yield moment;

$M_{u,t}$ = experimental ultimate moment;

$M_{cr,c}$ = predicted cracking moment;

$M_{y,c}$ = predicted yield moment;

$M_{u,c1}$ = predicted ultimate moment by using yield strength of steel reinforcement;

$M_{u,c2}$ = predicted ultimate moment by using ultimate strength of steel reinforcement;

ρ_s = reinforcement ratio.

References

[1] Victor C Li, Shuxin Wang, Cynthia Wu. Tensile strain-hardening behavior of PVA-ECC. ACI Mater. J., 98(6) (2001), pp. 483-492.

[2] Hezhi Liu, Qian Zhang,Chongshi Gu,Huaizhi Su, Victor Li. Self-healing of microcracks in Engineered Cementitious Composites under sulfate and chloride environment. Constr. Build. Mater., 153 (2017): pp. 948-956.

[3] Chung-Chan Hung, Yen-Fang Su. Medium-term self-healing evaluation of Engineered Cementitious Composites with varying amounts of fly ash and exposure durations. Constr. Build. Mater., 118 (2016): pp. 194-203.

[4] Chao Wu, V C Li. CFRP-ECC hybrid for strengthening of the concrete structures. Compos. Struct., 175(15) (2017): pp. 372-382.

[5] Erdoğan Özbay, Okan Karahan, Mohamed Lachemi, Cengiz Duran Atis. Dual effectiveness of freezing-thawing and sulfate attack on high-volume slag-incorporated ECC. Compos. Part B-Eng., 45(1) (2013): pp. 1384-1390.

[6] Hamid Reza Pakravan, Masoud Jamshidi, Masoud Latifi. Study on fiber hybridization effect of engineered cementitious composites with low-and high-modulus polymeric fibers. Constr. Build. Mater., 112 (2016): pp. 739-746.

[7] Hui Ma, Jingming Cai, Zhan Lin, Victor Li. $CaCO_3$ whisker modified Engineered Cementitious Composite with local ingredients. Constr. Build. Mater., 151 (2017): pp. 1-8.

[8] Junxia Li, En-Hua Yang. Macroscopic and microstructural properties of engineered cementitious composites incorporating recycled concrete fines. Cement Concrete Comp., 78(2017): pp. 33-42.

[9] Mustafa Şahmaran, Erdoğan Özbay, Hasan Erhan Yücel, Victor Li. Frost resistance and microstructure of Engineered Cementitious Composites: Influence of fly ash and micro poly-vinyl-alcohol fiber. Cement Concrete Comp., 34 (2) (2012): pp. 156-165.

[10] Jing Yu, Hedong Li, Christopher K.Y. Leung, Kaimin Shih. Matrix design for waterproof Engineered Cementitious Composites (ECCs). Constr. Build. Mater., 139 (2017): pp. 438-446.

[11] Shamsher Bahadur Singh, Madappa VR Sivasubramanian. Flexural response of ECC strengthened reinforced concrete beams. Indian Concrete J., 87(7) (2013): pp.35-44.

[12] Nan, Wang, Shi-lang Xu. Flexural response of reinforced concrete beams strengthened with post-poured ultra high toughness cementitious composites layer. J. Cent. South Univ., 18(3) (2011): pp.932-939.

[13] Mykolas Daugevičius, Juozas Valivonis, Tomas Skuturna, Vladimir Popov. RC Beams strengthened with HPFRCC: Experimental and numerical results. J. Civ. Eng. Manag., 22(2) (2016):pp.254-270.

[14] M Maalej, VC Li. Introduction of strain-hardening engineered cementitious composites in design of reinforced concrete flexural members for improved durability. ACI Struct. J., 92(2) (1995): pp.167-176.

[15] M Maalej, K S Leong. Engineered cementitious composites for effective FRP-strengthening of RC beams. Compos. Sci. Technol., 65(7-8) (2005): pp.1120-1128.

[16] M. Maalej, S.T. Quek, Faiz Uddin Ahmed Shaikh, K.S. Leong. Review of potential structural applications of hybrid fiber Engineered Cementitious Composites. Constr. Build. Mater., 36(11) (2012): pp. 216-227.

[17] Shilang Xu, Nan Wang, Qinghua Li. Experimental study on the flexural performance of concrete beam strengthened with ultra-high toughness cementitious composites. China Civil Eng. J., 43 (5) (2010): pp.17-22.

[18] Xiufang Zhang, Shilang Xu, Hedong Li. Theoretical analysis of flexural performance of plain concrete beams strengthened with ultra-high toughness cementitious composites. China Civil Eng. J., 43 (7) (2010): pp. 51-62.

[19] Jun Zhang, Christopher K Y Leung, Yin Nee Cheung. Flexural performance of layered ECC-concrete composite beam. Compos. Sci. Technol., 66(11-12) (2006): pp.1501-1512.

[20] Jun Zhang, Zhenbo Wang, Xianchun Ju, Zhenjie Shi. Simulation of flexural performance of layered ECC-concrete composite beam with fracture mechanics model. Eng. Fract. Mech., 131 (2014): pp. 419-438.

[21] Yi-Wei Lin, Derek Lawley, Liam Wotherspoon, Jason Ingham. Out-of-plane Testing of Unreinforced Masonry Walls Strengthened Using ECC Shotcrete. Struct., 7(2016):pp.33-42.

[22] S.B. Singh, Richa Patil, Pankaj Munjal. Study of flexural response of engineered cementitious composite faced masonry structures. Eng. Struct., 150(1) (2017):pp. 786-802.

[23] Ayoub Dehghani, Fariborz Nateghi-Alahi, Gregor Fischer. Engineered cementitious composites for strengthening masonry infilled reinforced concrete frames. Eng. Struct., 105 (2015):pp. 197-208.

[24] Rui Zhang, Koji Matsumoto, Takayoshi Hirata, Junichiro Niwa. Application of PP-ECC in beam–column joint connections of rigid-framed railway bridges to reduce transverse reinforcements. Eng. Struct., 86(2015):pp. 146-156.

[25] Salahuddin Qudah, M. Maalej. Application of Engineered Cementitious Composites (ECC) in interior beam-column connections for enhanced seismic resistance. Eng. Struct., 69(9) (2014):pp. 235-245.

[26] Shwan H. Said, Hashim Abdul Razak. Structural behavior of RC engineered cementitious composite (ECC) exterior beam–column joints under reversed cyclic loading. Constr. Build. Mater., 107 (2016): pp. 226-234.

[27] Shao-Bo Kang, Kang-Hai Tan, En-Hua Yang. Progressive collapse resistance of precast beam-column sub-assemblages with engineered cementitious composites. Eng. Struct., 98(2015):pp. 186-200.

[28] Hezhi Liu, Qian Zhang, Victor Li, Chongshi Gu. Durability study on engineered cementitious composites (ECC) under sulfate and chloride environment. Constr. Build. Mater., 133 (2017): pp. 171-181.

[29] Scott Muzenski, Ismael Flores Vivian, Konstantin Sobolev. Hydrophobic engineered cementitious composites for highway applications. Cement Concrete Comp., 57 (2012): pp. 68-74.

[30] Manish A. Kewalramani, Osama Mohamed, Zubair Imam Syed. Engineered Cementitious Composites for Modern Civil Engineering Structures in Hot Arid Coastal Climatic Conditions. Procedia Eng., 180(2017): pp. 767-774.

[31] Aiqin Zhao, Jinglei Yang, En-Hua Yang. Self-cleaning engineered cementitious composites. Cement Concrete Comp., 64(25) (2012): pp. 74-83.

[32] Shunzhi Qian, Victor Li, H. Zhang, G.A. Keoleian. Life cycle analysis of pavement overlays made with Engineered Cementitious Composites. Cement Concrete Comp., 35(1) (2013): pp. 78-88.

[33] China Academy of Building Research. Code for design of concrete structures GB50010-2010. Beijing: China Building Industry Press (2010).

[34] Fang Yuan, Jinlong Pan, C. K. Y. Leung. Flexural behaviors of ECC and concrete/ECC composite beams reinforced with basalt fiber-reinforced polymer, J. Compos. Constr., 17(5) (2013): pp. 591-602.

[35] Yun Xu , Jinlong Pan. Flexural behaviors of double-reinforced ECC beams. J. Southeast Univ., 29(1) (2013): pp. 66-72. (English Edition)

[36] China Academy of Building Research. Standard for test method of concrete structures GB 50152-2012. Beijing: China Building Industry Press (2012).

[37] China Academy of Building Research. Standard for test method of mechanical properties on ordinary concrete GB/T50081-2002. Beijing: China Building Industry Press (2003).

[38] General Administration of Quality Supervision, Inspection and Quarantine of the People's Republic of China. Metallic materials tensile testing at ambient temperature GB/T228-2002. Beijing: Standards press of China (2002).

[39] Biyuan Wang, Wenjie Ge, Jingjing Zhou, Dafu Cao. Preparation and mechanic behaviors of engineered cementitious composites. J. Yangzhou Univ. (Nat. Sci. Ed.), 18(3) (2015): pp. 64~69.